Structural and Functional Alterations of Skeletal Muscle Microvasculature in Dystrophin-Deficient mdx Mice.

Claire Latroche, Béatrice Matot, Aurea Martins-Bach, David Briand, Bénédicte Chazaud, Claire Wary, Pierre G Carlier, Fabrice Chrétien, Grégory Jouvion

Title: Structural and functional alterations of skeletal muscle microvasculature in dystrophin-deficient mdx mice

List of authors:

Claire Latroche[1,2,3,4], Béatrice Matot[5,6], Aurea Martins-Bach[5,6,7], David Briand[1], Bénédicte Chazaud[2,3,4,$], Claire Wary[5,6], Pierre G. Carlier[5,6], Fabrice Chrétien[1,4,8*] & Grégory Jouvion[1,4*]

Full affiliations of all authors:

[1]Institut Pasteur, Infection and Epidemiology department, Human Histopathology and Animal Models, Paris, France; [2]INSERM U1016, Institut Cochin, Paris, France; [3]CNRS UMR8104, Paris, France; [4]Paris Descartes University, PRES Sorbonne-Paris-Cité, Paris, France; [5]Institut de Myologie, NMR Laboratory, Paris, France; [6]CEA, I[2]BM, MIRCen, IdM, NMR Laboratory, Paris, France; [7]Laboratory of Muscle Proteins and Comparative Histology, Human Genome Research Center, Biosciences Institute, University of Sao Paulo, Brazil; [8]CH Sainte-Anne, Neuropathology Department, Paris, France.

*These authors contributed equally to this work.

[$]Present address: Centre de Génétique et de Physiologie Moléculaire et Cellulaire, Claude Bernard Lyon 1 University, Lyon, France; CNRS UMR5534, Paris, France

Number of text page: 38

Number of tables: 3

Number of figures: 8

Short running head: Microvascular alterations in mdx mice

Grant numbers and sources support: This work was supported by the DIM (Domaine d'intérêt majeur) STEM-Pôle "Stem cells and cell medicine", Région Ile-de-France, Association Française contre les Myopathies and institutional funding from Institut Pasteur.

Contact:

Fabrice Chrétien. Fax: +33 (0) 1 40 61 31 55. Tel: +33 (0) 1 40 61 31 44. Mail: fabrice.chretien@pasteur.fr

Institut Pasteur, Histopathologie Humaine et Modèles Animaux, 28 rue du Docteur Roux, 75015 Paris.

Conflict of interest statement:

The authors declare no conflict of interest.

ABSTRACT

Duchenne Muscular Dystrophy (DMD) is a progressive neuromuscular disease, caused by an absence of dystrophin, inevitably leading to death. Although muscle lesions are well characterised, blood vessel alterations that would have major impact on muscle regeneration, remain poorly understood. Our aim was to elucidate alterations of the vascular network organisation, taking advantage of $Flk1^{GFP/+}$ crossed with mdx mice (model for human DMD where all blood vessels express GFP) and functional repercussions using *in vivo* nuclear magnetic resonance (NMR), combining arterial spin labeling imaging of perfusion, and ^{31}P-spectroscopy of phosphocreatine kinetics. For the first time, our study focused on old (12 month-old) mdx mice, displaying marked chronic muscle lesions, very similar to the lesions observed in human DMD, in comparison to young-adult (3 month-old) mdx mice displaying only mild muscle lesions with no fibrosis. Using an original approach combining specific animal model, state of the art histology/morphometry techniques, and functional NMR, we demonstrated (i) that the microvascular system is almost normal in young-adult in contrast to old mdx mice, displaying marked microvessel alterations, and (ii) functional repercussions on muscle perfusion and bioenergetics after a hypoxic stress, that vary depending on stage of pathology. This original approach clarifies disease evolution and paves the way for setting up new diagnostic markers or therapeutic strategies.

INTRODUCTION

Duchenne muscular dystrophy (DMD) is the most frequent genetic neuromuscular disorder affecting 1:3500 school-age boys worldwide. This X-linked muscle disease is characterised by progressive skeletal muscle weakness and cardiomyopathy, leading to premature death generally because of respiratory and/or cardiac failure. The cause of DMD is the absence of dystrophin, a key component of the dystrophin-associated protein complex involved in the linkage between myofiber cytoskeleton and extracellular matrix. When linkage is disrupted, muscle fibers develop normally but are more susceptible to damage due to mechanical stretch. Despite presence of satellite cells (muscle stem cells) and successive regeneration attempts, myofibers undergo necrosis and are eventually replaced by connective and adipose tissue [1].

Muscle lesions in DMD have been widely investigated, with studies focusing principally on myofibers and/or satellite cells (SC). Although (i) skeletal muscle is one of the most vascularised tissues, (ii) endothelial cells are essential in muscle regeneration process, and (iii) dystrophin is expressed in endothelial/smooth muscle cells, disease impact on blood vessels and effect of blood vessel alteration in disease expression remain poorly understood. In recent years, interest in DMD vascular network has increased with primary focus on vasculature-related therapeutic strategies [2] such as methods to increase vasculature by modulating VEGF/VEGFR pathways [3]. These strategies were initially based on: (i) observation of "grouped necrosis" in muscles of DMD patients, *i.e.* simultaneous necrosis of contiguous myofibers, suggesting local failure in capillary blood supply and muscle ischemic necrosis [4], and (ii) membrane-associated nitric oxide synthase (NOS) deficiency in dystrophin-deficient muscle [5]. The hypothesis of an ischemic process has been strongly discussed, as other studies could not detect any vascular bed abnormality in DMD either

morphologically using electron microscopy [6] or physiologically by studying muscle blood flow [7-9]. More recent studies carried out in DMD patients confronted blood vessel alteration with tissue fibrosis. They suggested that endomysial fibrosis plays an essential role, causing an increase in capillary-to-myofiber distances, which impairs both muscle fiber mechanical function and gas exchanges [10]. Moreover, increased distances between capillaries and myofibers could potentially impede their reciprocal stimulation by soluble factors secreted during muscle repair [11].

Rare studies addressed the relevance of muscle vascular network in dystrophinopathy pathophysiology in animal models, focusing on muscle vascular density and characterisation of a possible hypoxic condition in dystrophic muscle. Part of these studies pointed to a decreased vascular density and an impaired angiogenesis in 6 week- to 6 month-old mdx mice [12-14] the dystrophin-deficient murine model of human DMD. However, contradictory results were also published in mdx mice, showing a higher hindlimb perfusion one week after femoral artery dissection and significant increase in arteriole length density in 2 month-old animals [15]. These discrepancies could be related in part to the effect of aging in disease progression; age appears to be an important parameter to consider when studying vascular changes [3]. Thus, involvement of blood vessels in the pathogenesis of dystrophy is still not completely understood.

In the present study, we investigated both structural organisation and *in vivo* function of vascular system in young-adult (3 month-old) mdx mice, displaying only moderate subacute muscle lesions with no fibrosis, and old (12 month-old) mdx mice, displaying marked muscle lesions with persistent inflammation and fibrosis [16], more relevant for the study of DMD pathophysiology in human. We used complementary morphological approaches based on genetically-modified mice that allowed for the first time to reconstruct the 3-dimensional

microvascular network in mdx mouse. These were confronted to innovative histological techniques and dynamic and non-invasive multiparametric and functional nuclear magnetic resonance (NMR).

MATERIAL AND METHODS

Mice

C57Bl/6J control mice were obtained from Charles River Laboratory (l'Arbresle, France), mdx-4Cv with C57Bl/6 background mice, model for human DMD, were kindly provided by Pr. Gherardi (Hôpital Henri Mondor, France), Flk-1$^{GFP/+}$ mice, in which green fluorescent protein (GFP) is targeted in vascular endothelial growth factor (VEGF) receptor-2 gene locus, exhibiting a bright GFP signal in all endothelial cells, were kindly provided by A. Medvinsky (Institute for Stem Cell Research, University of Edinburgh, UK), and Flk-1$^{GFP/+}$::mdx-4Cv mice were obtained by crossing Flk-1$^{GFP/+}$ with mdx-4Cv mice. Only male animals were used *i.e*. young-adults (3 month-old) or old (12 month-old).

Animals were housed in animal facilities of the Institut Pasteur licensed by the French Ministry of Agriculture and complying with European Union regulations. Protocols were approved by the Institut Pasteur Animal Experimentation Ethics Committee (01332.01).

Microvascular network organisation in three dimensions

Young-adult and old Flk-1$^{GFP/+}$ and Flk-1$^{GFP/+}$::mdx-4Cv mice were anesthetised with isoflurane inhalation (Forene, Abbott, Rungis, France) and killed by cervical dislocation. *Gastrocnemius* muscles were removed and imaging of vascular network was carried out in two conditions: thick cryo-sections or whole muscle. *Gastrocnemius* muscle was snap frozen

in liquid nitrogen-cooled isopentane before cryosectionning (100 µm-thick sections). Confocal acquisitions were performed using a spinning disk microscope (Leica, Wetzlar, Germany), laser femto-second was used: Chameleon Ultra, 20×/0.7 and 40x/0.75 objectives and a CoolSnap HQ2 camera. Optical slices were taken every 0.5 or 0.3 μm interval along the z-axis (80 μm).

For whole muscle conditions, images of *Gastrocnemius* blood vessels were obtained from the entire muscle using multi-photon scanner resonant confocal Leica TCS-SP5 with 20x/0.95 objective. Optical slices were taken every 0.5 μm along the z-axis.

Histological/Immunohistochemical analysis

Gastrocnemius muscles were collected from mice after NMR experiments, snap frozen in liquid nitrogen-cooled isopentane and kept at –80°C. Six different levels of 7 μm-thick sections were cut and stained with hematoxylin-eosin (HE) to describe histopathological modifications of muscle tissue, and Sirius red for visualisation of collagen. For immunohistochemistry analyses, muscle cryosections were incubated with antibodies directed against endothelial cells (anti-CD31; Pharmingen), satellite cells (anti-Pax7; DHSB, Iowa city, IA, USA), pericytes (anti-NG2; Millipore), smooth muscle cells (αSMA; Sigma) and basal lamina (anti-laminin; Sigma). Primary antibodies were incubated overnight at 4°C and revealed by cy3- or TRITC-labeled secondary antibodies (Jackson ImmunoResearch Laboratories).

Morphometric analysis

Two-dimension analysis was performed to evaluate distribution of muscle fiber diameter, percentage of centro- or peri-nucleated fibers, microvessel count and distribution around each myofiber using ImageJ (NIH, Bethesda, MD, USA) and NIS-Element (Nikon) softwares. At least 200 fibers were considered for each muscle.

Three-dimensional analysis was performed to evaluate organisation of vascular network. For each muscle, 10 z-stack image reconstructions were achieved on 80 to 150 μm-thick frozen sections. Analysis was carried out using IMARIS (ImarisBitplane, Zurich, Switzerland) software (quantification of vessel density, tortuosity, volume, anastomose count, diameter and distance between microvessels).

Quantitative RT-PCR

We used real-time PCR to determine the level of angiogenesis-related mRNA expression in young-adult and old mdx mice. Total *Gastrocnemius* muscle RNA was extracted using RNeasy Mini Kit (Qiagen). One µg of total RNA was reverse transcribed into first-strand cDNA using Superscript II Reverse Transcriptase (Life technologies). Quantitative PCR was carried out on StepOne Plus RealTime PCR system (Applied Biosystems, Carlsbad, CA, USA). Reaction mixtures had a final volume of 20 µl, consisting of 1 µl of cDNA, 10 µl of Sybr Green Master (Roche) and 10 µM of primers, listed in Table 1. After initial denaturation, amplification was performed at 95°C (10 s), 60°C (5 s), 72°C (10 s) for 45 cycles. Calculation of relative expression was determined by the StepOnePlus software (Applied Biosystems) and fold change was normalized to 18S rRNA housekeeping gene.

Nuclear Magnetic Resonance analysis

NMR experiments were performed on: 3 month-old mdx-4Cv (n=6) and control C57Bl/6J (n=9) and on 12 month-old mdx-4Cv (n=5) and control C57Bl/6J (n=7).

Hyperaemic response paradigm: To highlight differences between normal and altered muscles we classically applied a stress to increase the global need for perfusion. Ischemia-reperfusion stress was applied to the mouse left hindlimb which provokes maximal vasodilatation and limited resistance of arteries/arterioles [17] just after tourniquet release.

In practice, anaesthesia was induced with 4% isoflurane delivered in 1.5 L/min air and maintained with 1.75% isoflurane. During experiments, a water heating pad ensured a constant temperature of 37°C and breathing was monitored. After a 24 min NMR acquisition at rest (baseline), ischemia of the leg was induced by occlusion of femoral artery by two surgical threads placed around the thigh and pulled tight by application of a weight [17]. After 30 min of ischemia, the weight was instantly removed, inducing a hyperaemic response which was monitored over the next 30 min. During whole protocol, dynamic acquisitions of NMR scans of interleaved perfusion imaging and ^{31}P-spectroscopy (^{31}P-NMRS) were collected.

Multiparametric functional NMR (mpf-NMR) acquisitions. *In vivo* NMR experiments were conducted in a 4 Tesla Biospec system equipped with a 20 cm diameter 200 mT.m^{-1} gradient insert (BrukerBioSpin MRI GmbH, Ettlingen, Germany). Mice were placed supine in a 6 cm diameter, 12 cm length volume transmitter ^{1}H coil for whole-body signal excitation. An actively decoupled 2 cm diameter surface ^{1}H coil, positioned below the left calf, was used for image signal reception. Muscle metabolites were probed by a 10 mm ^{31}P saddle-shaped coil placed around the left leg.

As described in detail elsewhere [17, 18], Arterial Spin Labeling (ASL)-NMR imaging and ^{31}P-NMRS acquisitions were interleaved using the dedicated Bruker MultiScanControl software (BrukerBioSpin GmbH) in order to follow simultaneously and non-invasively: (i) muscle perfusion signal by SATuration-Inversion Recovery (SATIR) (time resolution: 10 sec), and (ii) mitochondrial activity by dynamic ^{31}P-NMRS (time resolution: 2.5 sec). In brief, ASL imaging is based on non-invasive alternate magnetic tagging of blood water spins to provide endogenous markers of muscle perfusion, measured in regions of interest (ROI) drawn in posterior compartment of the leg. Muscle bioenergetics and pH were assessed from ratios of energetic phosphates measurable by ^{31}P-NMRS at rest, *in vivo* mitochondrial oxidative capacity was directly assessed from the rate of creatine rephosphorylation at the end of ischemia, and intramuscular pH was calculated from chemical shift between phosphocreatine (PCr) and inorganic phosphate (Pi). A minimum of 50% PCr depletion at the end of ischemia was necessary to reliably measure dynamics for PCr recovery, and examinations which did not reach this threshold were rejected.

NMR perfusion analysis. Images were acquired after positive or negative labeling alternately. To avoid large vessels, ROI were drawn in the posterior compartment of the leg. Muscle perfusion f was calculated from the normalized difference between consecutive images according to the equation [19]:

$$f = -\lambda/T_{ev} \times ln\left[\left(M^+ - M^-\right)/\left(M^+ + M^-\right) \times \left(1 - exp(r_1 T_{ev})\right) + 1\right]$$

where r_1 is the longitudinal relaxation rate for muscle (measured by saturation-recovery acquisition for each mouse at the end of 30 minutes hyperaemic period), M^+ and M^- are the signals of positive and negative labelled perfusion images and λ is the blood-tissue partition coefficient (λ =0.9).

^{31}P-NMR Spectroscopy analysis. Successive ^{31}P Free Induction Decays were acquired throughout rest, ischemia and hyperaemia. ^{31}P-spectroscopy gives access to principal metabolites implicated in energetic metabolism such as phosphocreatine (PCr), the three α, β, γ ATP and inorganic phosphate (Pi). Signal intensity of these resonances is directly proportional to their concentrations, which allows the quantitative following of these metabolite variations.

At ischemia and recovery, PCr recovery was fitted by a mono-exponential function with a least mean squares algorithm and pH was calculated from the chemical shift δ_{Pi} between PCr and Pi according to the formula [20]:

$$pH = 6.75 + log\left[{(3.27 - \delta_{Pi})}/{(\delta_{Pi} - 5.69)}\right]$$

Statistics

Perfusion data were analysed by repeated measurements ANOVA. Analyses were performed with NCSS-2007 software (Kaysville, UT, USA). Group comparisons for perfusion parameters and phosphorus spectroscopy analysis were performed using Mann-Whitney test.

Statistical analysis of histological data was performed with GraphPad-Prism software (La Jolla, CA, USA). Fiber diameter repartition was evaluated by a chi-square test followed by a multi-t-test corrected for multiple comparisons using Holm-Sidak method. Same multi-t-test was used to evaluate capillary count/fiber repartition.

Statistical significance was taken at $p<0.05$ and p-values indicated on figures are *$p<0.05$, **$p<0.01$, and ***$p<0.001$. Numerical NMR and histological data are reported as mean±SD.

RESULTS

Microvessels were defined as the small blood vessels located at the periphery of myofibers, in the endomysium, displaying a diameter of less than 20 μm and a wall sometimes containing one layer of αSMA-expressing cells, thus including capillaries, terminal arterioles and terminal venules [21].

Young-adult Flk1$^{GFP/+}$::mdx mice display a normal microvascular network organisation but a mild decrease in terminal arteriole density.

Polyphasic subacute lesions, characterised by small inflammatory infiltrates and centrally nucleated fibers, were observed in *Gastrocnemius* muscle (Figure 1A-B). Surprisingly, these lesions had no impact on blood microvascular network organisation. In both Flk1$^{GFP/+}$ and Flk1$^{GFP/+}$::mdx mice, vascular network was indeed well organised with straight microvessels located along myofibers, parallel to each other with few anastomoses oriented perpendicularly to myofibers (Figure 1C-F). Microvessel diameter, measured using diameter of endothelial cell fluorescence, was similar in both groups (13-14 μm), as well as anastomose count (1,200-1,650 anastomoses/mm^3) (Figure 1G-H).

Immunofluorescence analyses did not detect any significant difference between young-adult wild-type and mdx mice (Figure 2). Both muscles displayed the same myofiber cross-section diameter, fiber size distribution, and microvessel density, quantified by microvessel count per fiber. No macrovascular modification was detected either (data not shown). To characterise further the microvascular network and identify terminal arterioles, we carried out an immunohistochemistry against αSMA, highlighting perivascular smooth muscle cells. We quantified a 26% loss of αSMA expression in mdx mice, suggesting a decrease in terminal arteriole density (Figure 3I, J, L). Collectively, these results highlighted a normal

microvascular network organisation in muscles of both groups, but a mild decrease in terminal arteriole density, in mdx mice.

Capillary-to-fiber perimeter exchange index (CFPE) has been used to calculate the contact surface area between capillaries and myofibers. It provides an indirect quantitative criterion to evaluate movement of oxygen from capillaries to muscle fibers [22]. CFPE index was not affected in young-adult mdx mice (Figure 2F).

As almost no alteration of the microvascular network was detected at the morphological level, we investigated the expression of angiogenesis-related mRNA (VEGF and its receptors Flk1 and Flt1, CD31, Ang1, Ang2 and Tie1, Tie2 receptors and nNOS) (Figure 4A). We did not observe any significant modification of these mRNA expression in young-adult mdx mice, suggesting no stimulation of the angiogenesis process. In contrast, nNOS expression was significantly decreased in young-adult mdx mice.

Similar pericyte density but increase in satellite cell count in young-adult mdx mice.

Using immunohistochemistry analysis, we focused on important partners of endothelial cells: pericytes and satellite cells. Concerning pericytes (NG2+ cells located at the periphery of blood vessels in muscle sections [23]), no difference in density per mm^2 was detected between wt (151.6±14.3 pericytes/mm^2, n=5) and mdx (154.3±21.2 pericytes/mm^2, n=5) mice (Figure 3I-K). Satellite cells (SC; Pax7+ cells) are in a close relationship with endothelial cells and coupling between myogenesis and angiogenesis takes place concomitantly during muscle regeneration [24]. In young-adult mdx mice, we demonstrated using immunofluorescence an increase in SC count per mm^2 (wt: 14.5±0.3 SC/mm^2, n=4; mdx: 29.7±3.5 SC/mm^2, n=6; $p<0.01$) and per fibre (wt: 0.04±0.01 SC/fibre, n=4; mdx: 0.07±0.01 SC/fibre, n=5; $p<0.05$), in comparison to wt (Figure 3A-D).

Muscle blood perfusion is modified in young-adult mdx mice.

In accordance with our previous observations, profiles of reactive hyperaemia were significantly different in mdx (n=6) and wt (n=9) mice (Figure 5A, $p<10^{-6}$ with ANOVA). The release of ischemia provoked an instantaneous increase of perfusion which was lower in wt mice (mdx: 78.7±27.1 ml/min/100 g; wt: 41.3±32.3 ml/min/100 g, 20 s post-release). In wt mice, this first perfusion peak was followed by a drop to reach a plateau around a value of 26.6±9.2 ml/min/100 g peaking at 270 s post-ischemia. In contrast, mdx muscle perfusion slightly increased to a mean perfusion value of 84.8±24.8 ml/min/100 g at 300 s post-ischemia and reduced to 26.3±25.9 ml/min/100 g only 850 s after stress release (Figure 5A). Moreover, the global volume repaid after ischemia was significantly higher in mdx mice (wt: 474.3±216.3 ml/100 g; mdx: 1017.0±369.2 ml/100 g, $p<0.05$). The response to ischemic stress was therefore different and enhanced in young-adult mdx mice while almost no morphological modification of microvessels was detected.

Muscle bioenergetics in young-adult mice (Table 2)**.**

At rest, mdx mice displayed a slightly higher Pi/PCr ratio compared to wt which reflects an increase in ADP concentration in dystrophic mice. In addition, a lower PCr/γATP ratio was observed in mdx mice, reflecting a decrease in metabolically functional muscle tissue.

The 30 min ischemic stress induced a higher Pi/PCr ratio in mdx mice while PCr depletion tended to be accelerated compared to wt (mdx: ΔPCr = 65±9%; wt: ΔPCr = 58±6%; p=0.09).

At reactive hyperaemia, release revealed a significant acceleration of PCr resynthesis rate in mdx mice compared to wt, reflecting higher mitochondrial ATP production in the mdx.

However, contrarily to wt, combined ^{31}P-NMRS and perfusion results showed a very tight correlation between time of rephosphorylation τPCr and various parameters reflecting perfusion: maximum perfusion (r^2= 0.66, p<0.05), time-perfusion integrals (r^2= 0.99, p<0.001 until 30 sec; r^2>0.93, p<0.01 until 150s) (Figure 6). In wt, none of the correlations between τPCr and perfusion were significant.

In summary, phosphate metabolism was accelerated during ischemia in 3 month-old mdx mice. At recovery, mitochondrial oxidative rephosphorylation was unexpectedly faster and perfusion was increased in comparison to age-matched control mice. Moreover, perfusion in mdx was directly related to mitochondrial ATP production. This is unlike normal healthy case where a luxury perfusion is observed and is neither limiting nor correlated to τPCr.

Alteration of microvascular network organisation in old Flk1$^{GFP/+}$::mdx mouse.

Old mdx mice displayed marked histological lesions; some already observed in young-adult as anisocytosis or centrally nucleated myofibers, others included persistence of chronic inflammation, and presence of endomysial/perimysial fibrosis (Figure 7A-D). The microvascular network was as well organised in old Flk1$^{GFP/+}$ as in young-adult mice (Figure 7E). In contrast, Flk1$^{GFP/+}$::mdx mice displayed significant alterations, characterised by a marked increase in tortuosity and irregular scattering of microvessels (Figure 7F). Microvessel diameter was similar in both groups (12 μm), but we identified a higher anastomose count, from more than 50,000 anastomoses/mm^3 for Flk1$^{GFP/+}$::mdx mice to less than 1,000 anastomoses/mm^3 for control Flk1$^{GFP/+}$ (p<0.01) (Figure 7J). Collectively, these results pointed to an anarchic blood vessel organisation in this context of dystrophinopathy.

Immunofluorescence analyses showed that (i) myofiber cross-section mean diameter was smaller in mdx mice (mdx: 47.4±4.2 μm; wt: 61.2±3.9 μm; p<0.001) (Figure 8C), (ii) the

smaller myofibers (<50μm) were clearly under-vascularised (Figure 8E), (iii) perinucleated (Figure 8G), and (iv) represented almost 60% of total muscle fibers in mdx mice in contrast to 35% in controls (Figure 8D). Alterations were also detected at the terminal arteriole level, as a loss of 70% of αSMA expression was detected in old mdx mice (wt: 88.6±2.4%, n=7; mdx: 18.0±2.1%, n=8; p<0.001), suggesting a marked decrease in terminal arteriole density (Figure 3M, N, P). These data suggested either a progressive degradation of tissue with no maintenance of microvascular network with time or a defect of neo-angiogenesis. The CFPE was not affected in old mice (Figure 8F).

Angiogenesis-related mRNA expression analysis revealed a collapse of VEGF expression and its decoy receptor Flt1 (Figure 4B). As observed in young-adult mice, nNOS was also significantly decreased in old mdx mice.

Collectively, these results pointed out severe alterations of microvessel organisation, especially around small/atrophic myofibers, associated with alteration of angiogenesis, suggesting chronic alteration of endothelial-myogenic cell interface.

Pericytes and satellite cells in old mdx mice.

The density of pericytes was similar between wt and mdx mice but, in contrast to young-adult mdx mice, a decrease in satellite cell count was observed for old mdx mice (wt: 12.4±0.6 SC/mm^2, n=8; mdx: 10.0±0.8 SC/mm^2, n=9; p<0.05) (Figure 3E-H).

Alteration of muscle perfusion in old mdx mice.

Despite severe alterations in mdx muscle microvascular network organisation, at rest, no difference in muscle perfusion was observed between mdx and wt mice (mdx: 12.09±5.90

ml/min/100 g; wt: 8.19±2.19 ml/min/100 g). After tourniquet release, rapid increase of perfusion was detected in muscles of the posterior hindlimb compartment; this increase was significantly lower in old mdx mice (mdx perfusion maximal value at 380 s post-ischemia: 60.5±39.3 ml/min/100 g; wt perfusion maximal value at 400 s post-ischemia: 106.1±38.1 ml/min/100 g, $p<0.05$), in contrast to what was seen in young-adult mice.

Analysis of variance of perfusion time-courses demonstrated differing profiles between wt and mdx mice ($p<10^{-4}$), with specific differences in the early phase of reperfusion. A similar initial peak of perfusion, as the one observed in young-adult wt mice, was detected in the old wt group, 20 s post-ischemia, but was absent in mdx mice (Figure 5B).

Thus at 12 months, both mdx and wt showed different profiles from young-adult animals (ANOVA, $p<10^{-6}$), and in contrast to wt and young-adult mdx, old mdx mice displayed a decrease in muscle perfusion and a modified perfusion profile after an ischemic stress.

Muscle bioenergetics in 12 month-old mice (Table 3)**.**

At rest, no difference in pH was observed between wt (n=7) and mdx (n=5) mice but hypoxic stress induced a significant acidosis in both groups ($p<0.005$), more pronounced in mdx (wt: $\Delta pH = 0.22\pm0.06$; mdx: $\Delta pH = 0.30\pm0.04$; $p<0.05$). Ischemia was associated with a significant increase in PCr depletion in old dystrophic mice compared to wt, though the difference in Pi/PCr ratio between the two groups was not significant. Unlike in young-adult mice, the rephosphorylation rate was comparable in both groups. Indeed τPCr was shorter in the old compared to the young-adult wt mice ($p<0.01$), but was unchanged with age in the mdx mice. Thus no alteration of oxidative capacities was observed in old mdx mice in response to hypoxic stress compared to age-matched control mice, despite reduced perfusion. In older mice (wt and mdx), no correlation was found between τPCr and perfusion variables.

DISCUSSION

Our study deciphers lesions of muscle microvascular network, in a model of dystrophinopathy, using combination of state of the art histology/morphometry techniques and totally non-invasive functional approach. This experimental paradigm, combining histopathology and mpf-NMR, clearly relevant for clinical diagnosis and research, allowed us to associate for the first time the fine 3D-alterations of muscle microvascular network with functional repercussions on muscle.

Concerning the animal model, previous studies used 6 week to 6 month-old mdx mice [12, 14, 25], which display very few chronic lesions with no fibrosis, in contrast to what happens in human [16]. We therefore worked on 12 month-old mdx mice, displaying persistence of endomysial inflammation and fibrosis, more representative of human DMD and thus more relevant for chronic myopathy and DMD pathophysiology study, in contrast to young-adult mdx mice displaying no chronic lesions. We demonstrated (i) strong alterations of microvascular network structure associated with reduced muscle perfusion in old mdx mice, (ii) functional increase in muscle perfusion and mitochondrial oxidative phosphorylation with normal microvascular network organisation in young-adult mdx mice, and (iii) a different impact of age on wild-type and mdx mouse muscles.

In young-adult and old wild-type mice, no alteration could be detected in muscle histology or microvascular network organisation. Perfusion is primarily regulated by smooth muscles that control blood flow distribution and capillary recruitment [26]. Capillary resistance, at rest, plays only a minor role in perfusion regulation. Using ischemia-reperfusion, we provoke maximal arteriolar dilatation in order to limit arteriolar resistance, and thus microvessel network becomes predominant in control of muscle perfusion [27]. Analysis of perfusion profiles

revealed the existence of a "peak" of perfusion in the first seconds after ischemia release, for young-adult and old wild-type mice. This initial "peak" suggests specific regulation of perfusion in early phase after ischemia release, probably coordinated by perivascular smooth muscles and/or pericytes [28].

Surprisingly and in contrast to previous studies describing decreased vascular density [12, 14], we did not detect any alteration in vascular network 3D-organisation in young-adult mdx mice. However, muscle post-ischemic perfusion was higher than in aged-match control mice, and time resolution of mpf-NMR allowed to demonstrate the absence of the initial "peak" of perfusion. In the same time, we also demonstrated a 26% loss of αSMA expression in young-adult mdx muscle (and more than 70% loss in old mdx), suggesting a drop in perivascular smooth muscle cells, responsible for part of these deleterious effects. It has indeed been demonstrated *in vivo* that the re-expression of dystrophin only in smooth muscle cells significantly ameliorates vasoregulation in mdx mice [29] confirming the importance of perivascular cells (smooth muscle for example) in blood flow regulation. One of the possible key factor is NO production alteration [30] or impairment of neuronal NO synthase (nNOS) [30-32], very probably explaining the significant decrease in nNOS expression both in young-adult and old mdx mice, in our study. Concerning pericytes, Yemisci *et al*. demonstrated in the brain, after a 2h ischemic stress, that pericytes remain contracted despite successful re-opening of blood flow, impairing microcirculatory reflow [28]. These experiments were carried out *ex vivo*, and no functional *in vivo* validation was done. Our data seem therefore to highlight functional alterations of smooth muscles and/or pericytes after ischemic stress. This alteration is severe enough to significantly impact perfusion profiles between control and mdx mice, and we are currently carrying out new experiments to better understand the effect of an absence of dystrophin in perivascular cells and their involvement in dystrophinopathy pathophysiology.

Old Flk1$^{GFP/+}$::mdx model allowed us to highlight disorganisation of microvascular network. A marked increase in microvessel tortuosity, an irregular scattering, and an increase in anastomose count were observed. Existence of these highly abundant anastomoses, suggests that "radial" as well as "longitudinal" (parallel to myofibers) blood flow is important, and in turn, that "longitudinal" flow is abnormally heterogeneous, microvessel longitudinal resistance being likely to vary a lot from microvessel to microvessel which would be the driven force for collateral flow.

Considering the close association between microvessels and myofibers, we demonstrated in old mdx mice that more than 60% of myofibres were atrophic with peripheral nuclei and displayed less microvessels at their periphery, resulting in a global undercapillarisation and loss of terminal arterioles. In parallel, NMR analysis revealed a two-fold decrease in perfusion after ischemia release. The significant decrease of microvessel (capillary and terminal arteriole) density around small myofibers is likely responsible for these functional alterations. Our data are thus in agreement with other studies demonstrating the effect of age on dystrophinopathy pathophysiology [15, 25]. Our hypothesis is that interaction between angiogenesis and myogenesis could be affected in old mdx mice; the increasingly scarce microvessels would provoke an alteration of myofiber regeneration that in turn could lead to impairment of remaining microvascular network support, maintaining a vicious circle. With this idea, we focused on the dynamic of satellite cell density in the muscle tissue. While SC density in young-adult mdx mice was increased, very probably because of the stimulation of muscle regeneration, it collapsed in old mdx mice, with pathology evolution, suggesting a worsening of the situation and an increase in the severity of chronic muscle lesions. Decline in SC number and activity has already been observed with age in mdx mice, in association with attenuated Notch signalling transduction [33]. Christov *et al*. already introduced the idea that angiogenesis and myogenesis are coupled during muscle regeneration, these processes

446 involving several growth factors, such as VEGF [24]. In our study, we also observed
447 modifications of VEGF and its receptor Flt1 expression profiles. Flt1 is the decoy receptor of
448 VEGF [34], acting as a negative regulator of endothelial cell growth and differentiation. A
449 previous study demonstrated that mdx mice knock out for the Flt1 receptor (mdx:Flt1$^{+/-}$)
450 presented an improved muscle histology associated with a better muscle perfusion and force
451 production compared to mdx mice [35]. These data underlines the link between vascular
452 remodelling and muscle regeneration, even in severe chronic diseases. Concerning VEGF, the
453 2-fold decreased expression, detected in old mdx mice, was in accordance with previous
454 studies demonstrating that treatment with VEGF strongly ameliorates mdx phenotype, with
455 improvement of functional parameters, increase in capillary density, improved muscle
456 regeneration, and decrease in interstitial fibrosis [36, 37]. Fibrosis is incidentally a key parameter
457 influencing perfusion, and is increased in DMD [10]. However, fibrosis might not be the most
458 limiting factor to perfusion, as it only represents 10% of old mdx mice muscle tissue in our
459 study. Moreover, distance between capillaries and myofibers, generally modified with
460 endomysial fibrosis [22], is similar between young-adult and old wild-type and mdx mice.
461 The *in vivo* increase of post-ischemic muscle perfusion with old age in wt animals was found
462 to be reproducible in different mouse strains, but no explanation is currently put forward,
463 while effect of aging on perfusion is still debated even in humans [38, 39].

464 In parallel to perfusion analysis, acquisition of ^{31}P-spectroscopy revealed moderate energetic
465 metabolism alterations, in agreement with previous literature, and contrarily to what might be
466 expected from alterations of enzymatic activities or defects of mitochondrial localization *in*
467 *vitro*. Compensatory mechanisms must thus exist in dystrophic muscle [40-42].

468 As for perfusion, anomalies in phosphorus metabolites in wild-type animals depended on age,
469 as already evoked in early studies of mdx metabolism [41, 43]. Anomalies at rest were more

marked in younger mdx: Pi/PCr reflecting resting ADP production was increased while PCr/ATP proportional to functional muscle was reduced (-11%), coherently with other reports [40-42] (-50% or more in DMD children [44]).

Unlike a recent study in 3 month-old mdx mice [45], where 10min ischemia was used as stress protocol, we found greater depletion after 30min ischemia in both young-adult and old mdx. During prolonged ischemia, two energetic pathways are activated to supply ATP demand: ATP-PCr system and glycolytic pathway. Production of ATP directly from PCr consumption is very small; it is therefore unlikely that PCr would be consumed to compensate for defective glycolytic pathway. The higher depletion observed in both young-adult and old mdx could more likely reflect a higher ATP demand to maintain ionic homeostasis.

Confrontation between perfusion and metabolic data obtained simultaneously by NMR revealed that despite strongly reduced perfusion in old mdx mice, oxidative metabolism was preserved, suggesting existence of a "luxury perfusion", *i.e.* reserve of perfusion that can be eliminated without impact on muscle physiology, as previously evidenced in a model of peripheral artery disease [46]. It generally explains the absence, or very loose correlation, between perfusion and PCr recovery rates in wt animals and in old mdx. This contrasts with the tight correlation between initial perfusion and τPCr of young-adult mdx mice, which display faster τPCr recovery and stronger perfusion than controls. Using optical spectroscopy to analyse myoglobin and haemoglobin oxygen desaturation in parallel to ^{31}P-NMRS, Percival observed strong uncoupling between ATP synthesis and O_2 consumption in 4 month-old mdx, dystrophic muscle producing 39% ATP less per O_2 consumed than controls [45]. We might thus hypothesize that at this young age, increased perfusion might be a means to compensate for mitochondrial inefficiency.

In conclusion, we demonstrated strong structural and functional alterations in muscle microvascular network of dystrophin-deficient mdx mice, with an increasing severity in parallel to aging. Our approach combining 3D-morphological analyses with non-invasive functional evaluation, allowed to better characterise the impact of histological lesions on tissue function. Collectively, our data pointed out that vascular network has a key role in dystrophinopathy pathophysiology and would be very important target for the set-up of new innovative therapeutic strategies.

ACKNOWLEDGEMENTS

We thank Pr Romain Gherardi and Pr Jérôme Authier (Hôpital Henri Mondor), and Pr Shahragim Tajbakhsh (Institut Pasteur) for the scientific exchanges on muscle dystrophy pathophysiology, regeneration mechanisms and experimental devices. We also thank Dr Aurélien Mazeraud and Dr Anne Danckaert (Institut Pasteur) for the precious help in biostatistical analyses and Patricia Flamant for her technical support. This work was supported by the DIM (Domaine d'intérêt majeur) STEM-Pôle "Stem cells and cell medicine", Région Ile-de-France and Association Française contre les Myopathies (CL).

Statement of author contributions:

GJ, FC, CW, CL and PGC designed experiments. CL, BM, AMB and DB carried out experiments and GJ, FC, PGC, CW, BM and CL analysed data. GJ, CL, BC, BM and CW were involved in writing the paper and all authors gave final approval of the submitted and published versions.

List of abbreviations:

ADP: Adenosine diphosphate, ASL: Arterial spin labeling, ATP: Adenosine triphosphate, CFPE: capillary to fiber perimeter exchange, DMD: Duchenne muscular dystrophy, GFP: green fluorescent protein, HE: haematoxylin and eosin, NMR: nuclear magnetic resonance, NOS: nitric oxide synthase, PCr: Phosphocreatine, Pi: phosphate inorganic, SATIR: SATuration-Inversion Recovery, VEGF/R: vascular endothelial growth factor/Receptor

REFERENCES

1. De Paepe B, De Bleecker JL: Cytokines and chemokines as regulators of skeletal muscle inflammation: presenting the case of Duchenne muscular dystrophy, Mediators Inflamm 2013, 2013:540370
2. Ennen JP, Verma M, Asakura A: Vascular-targeted therapies for Duchenne muscular dystrophy, Skelet Muscle 2013, 3:9
3. Shimizu-Motohashi Y, Asakura A: Angiogenesis as a novel therapeutic strategy for Duchenne muscular dystrophy through decreased ischemia and increased satellite cells, Front Physiol 2014, 5:50
4. Engel WK, Hawley RJ: Focal lesions of muscle in peripheral vascular disease, J Neurol 1977, 215:161-168
5. Rando TA: Role of nitric oxide in the pathogenesis of muscular dystrophies: a "two hit" hypothesis of the cause of muscle necrosis, Microsc Res Tech 2001, 55:223-235
6. Koehler J: Blood vessel structure in Duchenne muscular dystrophy. I. Light and electron microscopic observations in resting muscle, Neurology 1977, 27:861-868
7. Bradley WG, O'Brien MD, Walder DN, Murchison D, Johnson M, Newell DJ: Failure to confirm a vascular cause of muscular dystrophy, Arch Neurol 1975, 32:466-473
8. Gudrun B, Andrew GE, Boysen G, Engel AG: Effects of microembolization on the skeletal muscle blood flow. A critique of the microvascular occlusion model of Duchenne dystrophy, Acta Neurol Scand 1975, 52:71-80
9. Leinonen H, Juntunen J, Somer H, Rapola J: Capillary circulation and morphology in Duchenne muscular dystrophy, Eur Neurol 1979, 18:249-255
10. Desguerre I, Mayer M, Leturcq F, Barbet J-P, Gherardi RK, Christov C: Endomysial fibrosis in Duchenne muscular dystrophy: a marker of poor outcome associated with

547 macrophage alternative activation, Journal of Neuropathology & Experimental
548 Neurology 2009, 68:762-773
549 11. Christov C, Chretien F, Abou-Khalil R, Bassez G, Vallet G, Authier FJ, Bassaglia Y,
550 Shinin V, Tajbakhsh S, Chazaud B, Gherardi RK: Muscle satellite cells and
551 endothelial cells: close neighbors and privileged partners, Mol Biol Cell 2007,
552 18:1397-1409
553 12. Loufrani L: Absence of Dystrophin in Mice Reduces NO-Dependent Vascular
554 Function and Vascular Density: Total Recovery After a Treatment with the
555 Aminoglycoside Gentamicin, Arterioscler Thromb Vasc Biol 2004, 24:671-676
556 13. Landisch RM, Kosir AM, Nelson SA, Baltgalvis KA, Lowe DA: Adaptive and
557 nonadaptive responses to voluntary wheel running by mdx mice, Muscle Nerve 2008,
558 38:1290-1303
559 14. Matsakas A, Yadav V, Lorca S, Narkar V: Muscle ERRgamma mitigates Duchenne
560 muscular dystrophy via metabolic and angiogenic reprogramming, Faseb J 2013,
561 27:4004-4016
562 15. Straino S: Enhanced Arteriogenesis and Wound Repair in Dystrophin-Deficient mdx
563 Mice, Circulation 2004, 110:3341-3348
564 16. Grounds MD, Radley HG, Lynch GS, Nagaraju K, De Luca A: Towards developing
565 standard operating procedures for pre-clinical testing in the mdx mouse model of
566 Duchenne muscular dystrophy, Neurobiol Dis 2008, 31:1-19
567 17. Bertoldi D, Loureiro de Sousa P, Fromes Y, Wary C, Carlier PG: Quantitative,
568 dynamic and noninvasive determination of skeletal muscle perfusion in mouse leg by
569 NMR arterial spin-labeled imaging, Magn Reson Imaging 2008, 26:1259-1265

570 18. Baligand C, Gilson H, Menard JC, Schakman O, Wary C, Thissen JP, Carlier PG:
571 Functional assessment of skeletal muscle in intact mice lacking myostatin by
572 concurrent NMR imaging and spectroscopy, Gene Ther 2010, 17:328-337
573 19. Raynaud JS, Duteil S, Vaughan JT, Hennel F, Wary C, Leroy-Willig A, Carlier PG:
574 Determination of skeletal muscle perfusion using arterial spin labeling NMRI:
575 validation by comparison with venous occlusion plethysmography, Magn Reson Med
576 2001, 46:305-311
577 20. Taylor DJ, Bore PJ, Styles P, Gadian DG, Radda GK: Bioenergetics of intact human
578 muscle. A 31P nuclear magnetic resonance study, Mol Biol Med 1983, 1:77-94
579 21. Granger DN, Senchenkova E: Edited by San Rafael (CA), 2010, p.
580 22. Hepple RT: A new measurement of tissue capillarity: the capillary-to-fibre perimeter
581 exchange index, Can J Appl Physiol 1997, 22:11-22
582 23. Wanjare M, Kusuma S, Gerecht S: Perivascular cells in blood vessel regeneration,
583 Biotechnol J 2013, 8:434-447
584 24. Christov C, Chretien F, Abou-Khalil R, Bassez G, Vallet Gg, Authier Fo-Jrm,
585 Bassaglia Y, Shinin V, Tajbakhsh S, Chazaud Bnd, others: Muscle satellite cells and
586 endothelial cells: close neighbors and privileged partners, Mol Biol Cell 2007,
587 18:1397-1409
588 25. Palladino M, Gatto I, Neri V, Straino S, Smith RC, Silver M, Gaetani E, Marcantoni
589 M, Giarretta I, Stigliano E, Capogrossi M, Hlatky L, Landolfi R, Pola R: Angiogenic
590 impairment of the vascular endothelium: a novel mechanism and potential therapeutic
591 target in muscular dystrophy, Arterioscler Thromb Vasc Biol 2013, 33:2867-2876
592 26. Clifford PS: Vasodilatory mechanisms in contracting skeletal muscle, J Appl Physiol
593 (1985) 2004, 97:393-403

27. Baligand C, Jouvion G, Schakman O, Gilson H, Wary C, Thissen JP, Carlier PG: Multiparametric functional nuclear magnetic resonance imaging shows alterations associated with plasmid electrotransfer in mouse skeletal muscle, J Gene Med 2012, 14:598-608

28. Yemisci M, Gursoy-Ozdemir Y, Vural A, Can A, Topalkara K, Dalkara T: Pericyte contraction induced by oxidative-nitrative stress impairs capillary reflow despite successful opening of an occluded cerebral artery, Nat Med 2009, 15:1031-1037

29. Ito K: Smooth muscle-specific dystrophin expression improves aberrant vasoregulation in mdx mice, Hum Mol Genet 2006, 15:2266-2275

30. Loufrani L, Matrougui K, Gorny D, Duriez M, Blanc I, Levy BI, Henrion D: Flow (shear stress)-induced endothelium-dependent dilation is altered in mice lacking the gene encoding for dystrophin, Circulation 2001, 103:864-870

31. Brenman JE, Chao DS, Xia H, Aldape K, Bredt DS: Nitric oxide synthase complexed with dystrophin and absent from skeletal muscle sarcolemma in Duchenne muscular dystrophy, Cell 1995, 82:743-752

32. Sander M, Chavoshan B, Harris SA, Iannaccone ST, Stull JT, Thomas GD, Victor RG: Functional muscle ischemia in neuronal nitric oxide synthase-deficient skeletal muscle of children with Duchenne muscular dystrophy, Proc Natl Acad Sci U S A 2000, 97:13818-13823

33. Jiang C, Wen Y, Kuroda K, Hannon K, Rudnicki MA, Kuang S: Notch signaling deficiency underlies age-dependent depletion of satellite cells in muscular dystrophy, Disease Models & Mechanisms 2014, 7:997-1004

34. Fong GH, Rossant J, Gertsenstein M, Breitman ML: Role of the Flt-1 receptor tyrosine kinase in regulating the assembly of vascular endothelium, Nature 1995, 376:66-70

35. Verma M, Asakura Y, Hirai H, Watanabe S, Tastad C, Fong GH, Ema M, Call JA, Lowe DA, Asakura A: Flt-1 haploinsufficiency ameliorates muscular dystrophy phenotype by developmentally increased vasculature in mdx mice, Hum Mol Genet 2010, 19:4145-4159

36. Deasy BM, Feduska JM, Payne TR, Li Y, Ambrosio F, Huard J: Effect of VEGF on the regenerative capacity of muscle stem cells in dystrophic skeletal muscle, Mol Ther 2009, 17:1788-1798

37. Messina S, Mazzeo A, Bitto A, Aguennouz M, Migliorato A, De Pasquale MG, Minutoli L, Altavilla D, Zentilin L, Giacca M, Squadrito F, Vita G: VEGF overexpression via adeno-associated virus gene transfer promotes skeletal muscle regeneration and enhances muscle function in mdx mice, Faseb J 2007, 21:3737-3746

38. Trinity JD, Layec G, Lee JF: Heterogeneity of blood flow: impact of age on muscle specific tissue perfusion during exercise, J Physiol 2014, 592:1729-1730

39. Rudroff T, Weissman JA, Bucci M, Seppanen M, Kaskinoro K, Heinonen I, Kalliokoski KK: Positron emission tomography detects greater blood flow and less blood flow heterogeneity in the exercising skeletal muscles of old compared with young men during fatiguing contractions, J Physiol 2014, 592:337-349

40. Cole MA, Rafael JA, Taylor DJ, Lodi R, Davies KE, Styles P: A quantitative study of bioenergetics in skeletal muscle lacking utrophin and dystrophin, Neuromuscul Disord 2002, 12:247-257

41. Dunn JF, Frostick S, Brown G, Radda GK: Energy status of cells lacking dystrophin: an in vivo/in vitro study of mdx mouse skeletal muscle, Biochim Biophys Acta 1991, 1096:115-120

42. Heerschap A, Bergman AH, van Vaals JJ, Wirtz P, Loermans HM, Veerkamp JH: Alterations in relative phosphocreatine concentrations in preclinical mouse muscular dystrophy revealed by in vivo NMR, NMR Biomed 1988, 1:27-31

43. Dunn JF, Tracey I, Radda GK: Exercise metabolism in Duchenne muscular dystrophy: a biochemical and [31P]-nuclear magnetic resonance study of mdx mice, Proc Biol Sci 1993, 251:201-206

44. Kemp GJ, Taylor DJ, Dunn JF, Frostick SP, Radda GK: Cellular energetics of dystrophic muscle, J Neurol Sci 1993, 116:201-206

45. Percival JM, Siegel MP, Knowels G, Marcinek DJ: Defects in mitochondrial localization and ATP synthesis in the mdx mouse model of Duchenne muscular dystrophy are not alleviated by PDE5 inhibition, Hum Mol Genet 2013, 22:153-167

46. Vidal G WC, Giacomini E, Emmanuel F, Carlier PG: A truly non-invasive set-up for the study of perfusion and energy metabolism in the rat calf in vivo: application to a model of peripheral arterial disease (Abstract), Magma 2002, 25:15

FIGURE LEGENDS

FIGURE 1. Normal microvascular network organisation in 3 month-old mdx mice.

In contrast to wild-type mice (A), mdx mice (B) display subacute lesions in *Gastrocnemius* muscle, characterised by small inflammatory infiltrates (star) associated with regenerated myofibers displaying central nuclei (arrows) (HE staining).

Microvessel 3D organisation of $Flk1^{GFP/+}$ (C,E) and $Flk1^{GFP/+}$::mdx (D,F) mice: normal blood microvessel organisation, with microvessels regularly scattered along myofibers (C-F) (Scale bars: 50 μm). Morphometric analyses revealed similar diameter (G) and anastomose count/mm^3 (H) between microvessels from wild-type and mdx mice.

FIGURE 2. Microvessel morphometry in 3 month-old mice.

Young-adult wild-type (n=5) and mdx (n=3) mice display similar: microvessel distribution in *Gastrocnemius* muscle (A,B) (laminin-FITC and CD31-TRITC immunohistochemistry to label basal lamina (green) and blood vessels (red); Scale bar: 50 μm), fiber size repartition (C), microvessel count per fiber (D), microvessel diameter (E), and capillary to fiber perimeter exchange index (CFPE) (F).

FIGURE 3. Satellite cells, terminal arterioles and pericytes are affected in mdx mice.

Pool of SC was analysed by immunohistochemistry (A, B, E, F, white arrows) (Pax7-FITC and Laminin-Cy3). SC density is increased in young-adult mdx mice (C, D) while we observed a significant depletion of the SC pool in old mdx mice (G, H). Pericyte density, assessed using NG2 immunolabeling (NG2-FITC), was similar for all groups, at all ages (I-

K, M-O). We also evaluated the expression of αSMA (Smooth Muscle Actin) by perivascular smooth muscle cells, surrounding terminal arterioles (αSMA-Cy3). We observed a decrease of 26% αSMA expression for young-adult mdx mice in comparison to wt animals (I, J, L), reaching 70% loss for old mdx (M, N, P), suggesting a marked drop in terminal arterioles, increasing with the disease progression (scale bars: 25 μm) (*p<0.05, **p<0.01, ***p<0.001).

FIGURE 4. Analysis of angiogenesis-related gene expression by RT-qPCR.

Total RNA was extracted and complementary DNA was analysed by qPCR. Gene expression was measured in the *Gastrocnemius* of young-adult (A) and old (B) mdx mice. Results were normalized relative to the expression of the 18s rRNA housekeeping gene. Data are presented as fold change mean±SEM. Symbol ** indicates statistical difference (p<0.01) observed between mdx and wild-type mice from the same age.

FIGURE 5. Muscle blood perfusion during ischemia-reperfusion.

After release of ischemia, a rapid and important increase in perfusion is detected.

(A) Different profiles of perfusion are obtained in young-adult mice: total perfusion is higher in mdx mice and a first "peak" of perfusion followed by a rapid decrease in muscle perfusion is only detected in wild-type mice.

(B) A first "peak", similar to what is observed in young-adult wild-type mice, is also observed in 12 month-old control animals. This first "peak" does not exist in mdx mice that

701 also displayed a reduced perfusion, with a maximum perfusion equivalent to half the value
702 observed in wild-type mice during the hyperaemia phase.

703 As the release of ischemia induced movements of the leg, images affected by these
704 movement artefacts are removed from analysis of muscle perfusion.

705

706 **FIGURE 6.** Correlation between perfusion and time of creatine rephosphorylation (τPCr) in
707 3 month-old mice.

708 Correlation between τPCr and maximal perfusion (A) or time-perfusion integrals until 30 sec
709 (B) is significant in mdx mice (*$p<0.05$ and ***$p<0.001$, respectively) with a coefficient of
710 determination r^2 of 0.66 and 0.99, respectively. In wt, none of the correlations were
711 significant.

712

713 **FIGURE 7.** Alteration of microvascular network in 12 month-old mdx mice.

714 Twelve month-old wild-type mice display histologically normal muscles (A), with no fibrosis
715 (C), and regularly scattered microvessels along myofibers, with few anastomoses (E,G,J). In
716 contrast, 12 month-old mdx mice display chronic histological lesions (B), characterised by
717 multifocal inflammatory infiltrates (mostly macrophages), included in endomysial collagen
718 tissue (fibrosis; stars), associated with a marked variation in myofiber size (anisocytosis) and
719 the presence of atrophic and regenerating myofibers displaying centrally-located nuclei
720 (arrows). Sirius red staining and fluorescence microscopy reveal a moderate to marked
721 endomysial fibrosis (D) and microvascular network alterations (F,H), characterised by
722 irregularly scattered tortuous microvessels (Scale bars: 50 μm). Even if microvessel diameter
723 is similar between mdx and wild-type mice (I), a clear increase in anastomose count/mm^3 is

724 detected for old mdx mice (J). A, B: HE staining. C, D: Sirius red staining (specific for
725 collagen staining). **p<0.01.

726

727 **FIGURE 8.** Twelve month-old mdx mice display atrophic myofibers with low capillarisation
728 and terminal arteriole density.

729 Anisocytosis is more pronounced in old mdx mice, with the presence of small atrophic
730 myofibers (A-C) (Laminin-FITC and CD31-TRITC immunohistochemistry; Scale bars: 50
731 μm). Atrophic myofibers (with a diameter up to 60 μm) represent more than 60% of the total
732 myofibers in mdx mice (D). These atrophic myofibers display less microvessels at their
733 periphery (E). The distance between microvessels and myofibers, calculated using the
734 capillary to fiber perimeter exchange index (CFPE) is similar in both groups (F). Small
735 myofibers with low capillarisation are mostly perinucleated myofibers (G) (**p<0.01,
736 ***p<0.001).

737

738

TABLES

Table 1. Oligonucleotide Primers Used for qPCR

Primer	Sequence
18S rRNA F	5'-CGGACAGGATTGACAGATTG-3'
18S rRNA R	5'-CAAATCGCTCCACCAACTAA-3'
Flk1 F	5'-CAGTGGTACTGGCAGCTAGAAG-3'
Flk1 R	5'-ACAAGCATACGGGCTTGTTT-3'
Flt1 F	5'-GGCCCGGGATATTTATAAGAAC-3'
Flt1 R	5'-CCATCCATTTTAGGGGAAGTC-3'
VEGF F	5'-GGCGTGGTGGTGACATGGTT-3'
VEGF R	5'-ACCTCACCAAAGCCAGCACA-3'
CD31 F	5'-CGGTGTTCAGCGAGATCC-3'
CD31 R	5'-ACTCGACAGGATGGAAATCAC-3'
Ang1 F	5'-GACAGTAATACAACACCGGGAAGA-3'
Ang1 R	5'-CAAAACCCATTTTATACTCCTTCCA-3'
Ang2 F	5'-ACTACGACGACTCAGTGCAAAG-3'
Ang2 R	5'-TCTGGTTCTGCACCACATTC-3'
Tie1 F	5'-AGGGCAGCTTCCAGAGTATG-3'

Tie1 R	5'-GGTTGGCCAGCAATGTTAAG-3'
Tie2 F	5'-GGCTATAAGGATACGGACCATGAA-3'
Tie2 R	5'-TCCCCTGTCCACGGTCATA-3'
nNOS F	5'-GGCGTTCGTGATTACTGTGA-3'
nNOS R	5'-TCTTCCTCATGTCCAAATCCA-3'

741

742

743 Table 2. Energetic metabolism analysis from ^{31}P-spectroscopy in young-adult mice.

	wt (n=9)	**mdx (n=6)**
ΔPCr (%)	58 ± 6	65 ± 9
τPCr (s)	118 ± 34	76 ± 34*
pH at rest (pH_{rest})	7.20 ± 0.04	7.17 ± 0.03
pH end ischemia (pH_{end})	7.00 ± 0.08	6.98 ± 0.03
Pi/PCr at rest (Pi/PCr_{rest})	0.08 ± 0.03	0.10 ± 0.01*
Pi/PCr end ischemia (Pi/PCr_{end})	0.93 ± 0.25	1.71 ± 0.52*
PCr/ATPγ at rest ($PCr/ATP\gamma_{rest}$)	3.39 ± 0.25	3.01 ± 0.27*
PCr/ATPγ end ischemia ($PCr/ATP\gamma_{end}$)	1.80 ± 0.62	1.39 ± 0.51

744

745 Ischemia stress was sufficient as the mean depletion of phosphocreatine (PCr) for wt and
746 mdx mice was above 50%. Pi/PCr at rest and after ischemia were higher in mdx compared to
747 wt mice while PCr/ATPγ at rest was lower (*$p<0.05$).

748

749 Table 3. Energetic metabolism analysis from ^{31}P-spectroscopy in old mice.

	wt (n=7)	**mdx (n=5)**
ΔPCr (%)	54 ± 4	63 ± 2**
τ PCr (s)	66 ± 25	80 ± 20
pH at rest (pH_{rest})	7.16 ± 0.07	7.18 ± 0.04
pH end ischemia (pH_{end})	6.94 ± 0.04	6.87 ± 0.04*
Pi/PCr at rest (Pi/PCr_{rest})	0.08 ± 0.04	0.10 ± 0.01
Pi/PCr end ischemia (Pi/PCr_{end})	1.24 ± 0.40	1.34 ± 0.20
PCr/ATPγ at rest ($PCr/ATP\gamma_{rest}$)	2.98 ± 0.35	3.05 ± 0.16
PCr/ATPγ end ischemia ($PCr/ATP\gamma_{end}$)	1.20 ± 0.35	1.36 ± 0.30

750

751 Ischemia stress was sufficient as the mean depletion of phosphocreatine (PCr) for wt and
752 mdx mice was above 50%. ΔPCr is higher in mdx mice; pH decreased for both wt and mdx
753 mice after ischemia, but mdx mice suffered a more severe acidosis. Others energetic
754 parameters did not change in our experimental conditions (*p<0.05, **p<0.01).

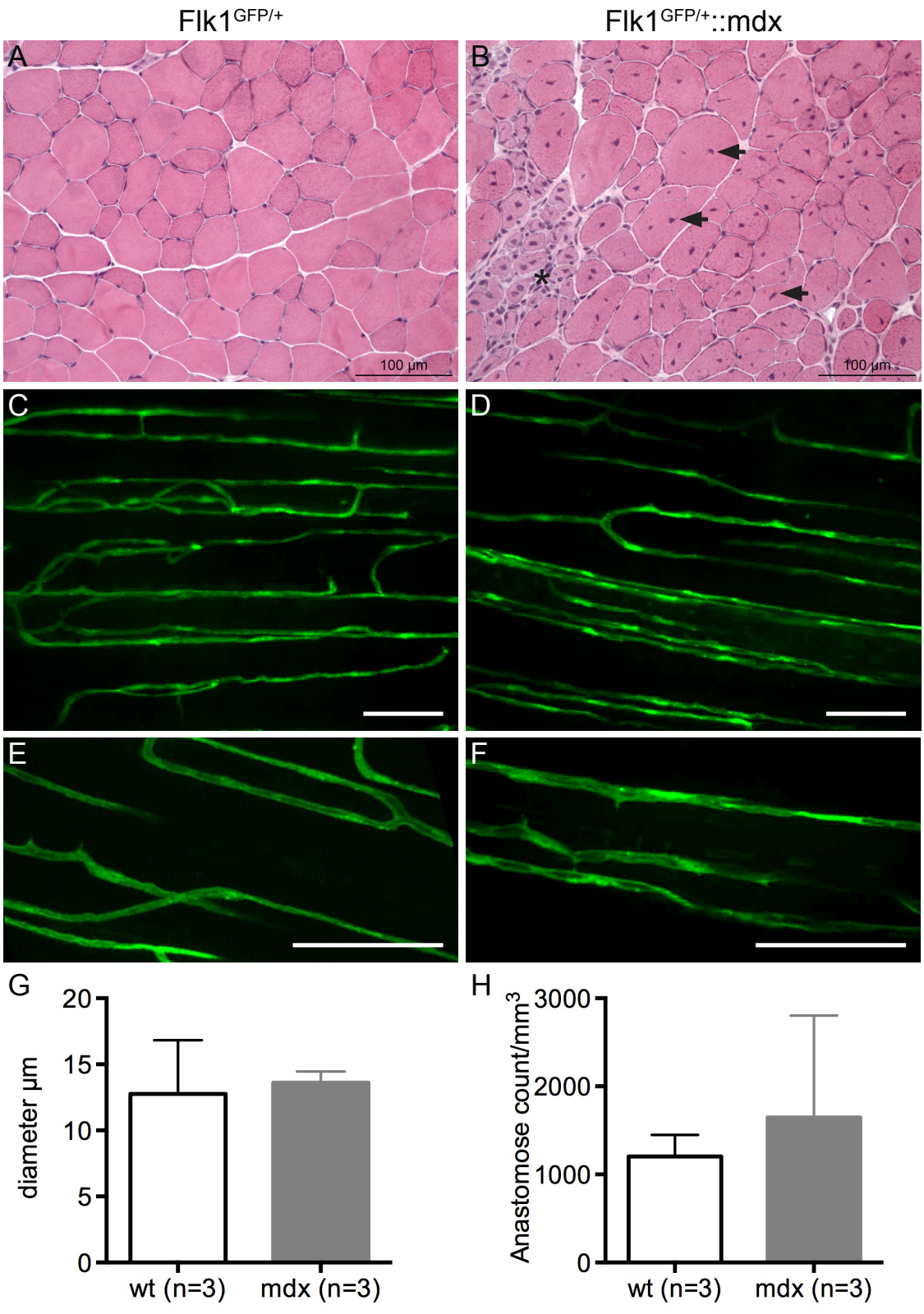
Flk1GFP/+
Flk1GFP/+::mdx
A
B
100 µm
100 µm
C
D
E
F
G
diameter µm
20
15
10
5
0
wt (n=3)
mdx (n=3)
H
Anastomose count/mm3
3000
2000
1000
0
wt (n=3)
mdx (n=3)

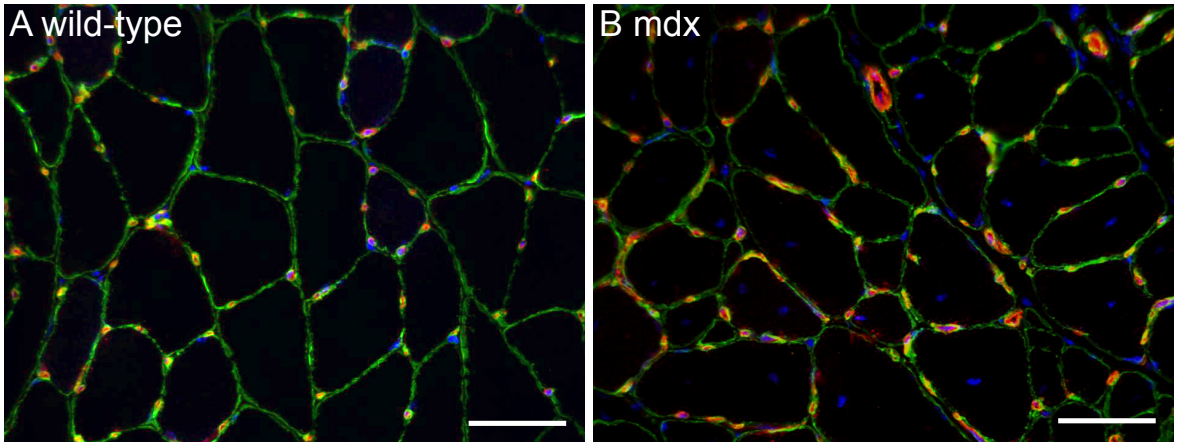
A wild-type
B mdx

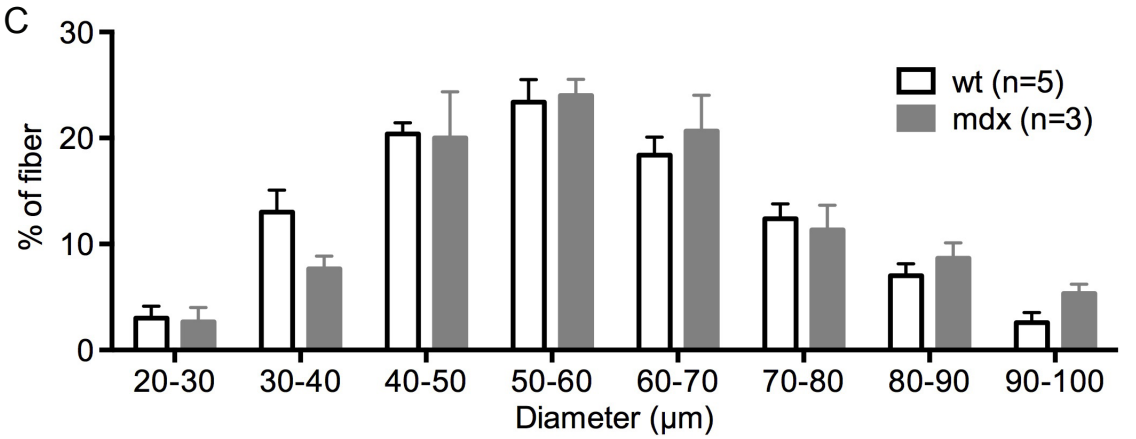
C
% of fiber
30
20
10
0
wt (n=5)
mdx (n=3)
20-30
30-40
40-50
50-60
60-70
70-80
80-90
90-100
Diameter (µm)

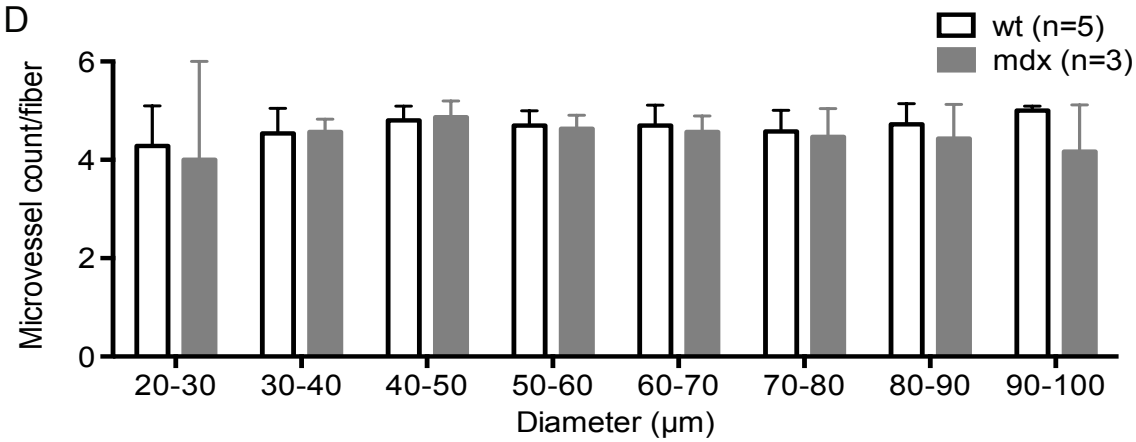
D
Microvessel count/fiber
6
4
2
0
wt (n=5)
mdx (n=3)
20-30
30-40
40-50
50-60
60-70
70-80
80-90
90-100
Diameter (µm)

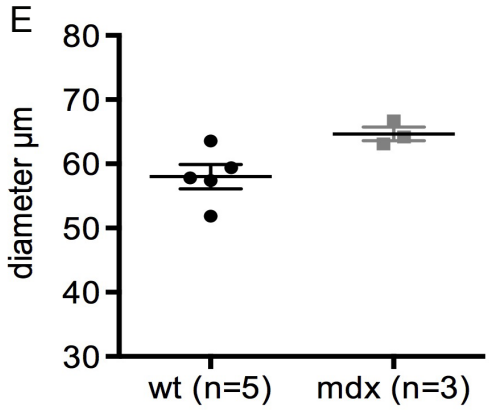
E
diameter µm
80
70
60
50
40
30
wt (n=5)
mdx (n=3)

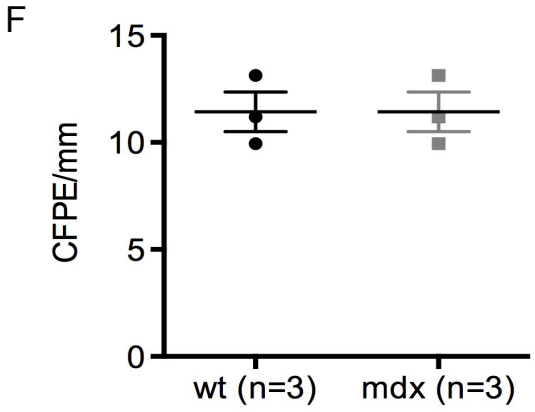
F
CFPE/mm
15
10
5
0
wt (n=3)
mdx (n=3)

Satellite cells

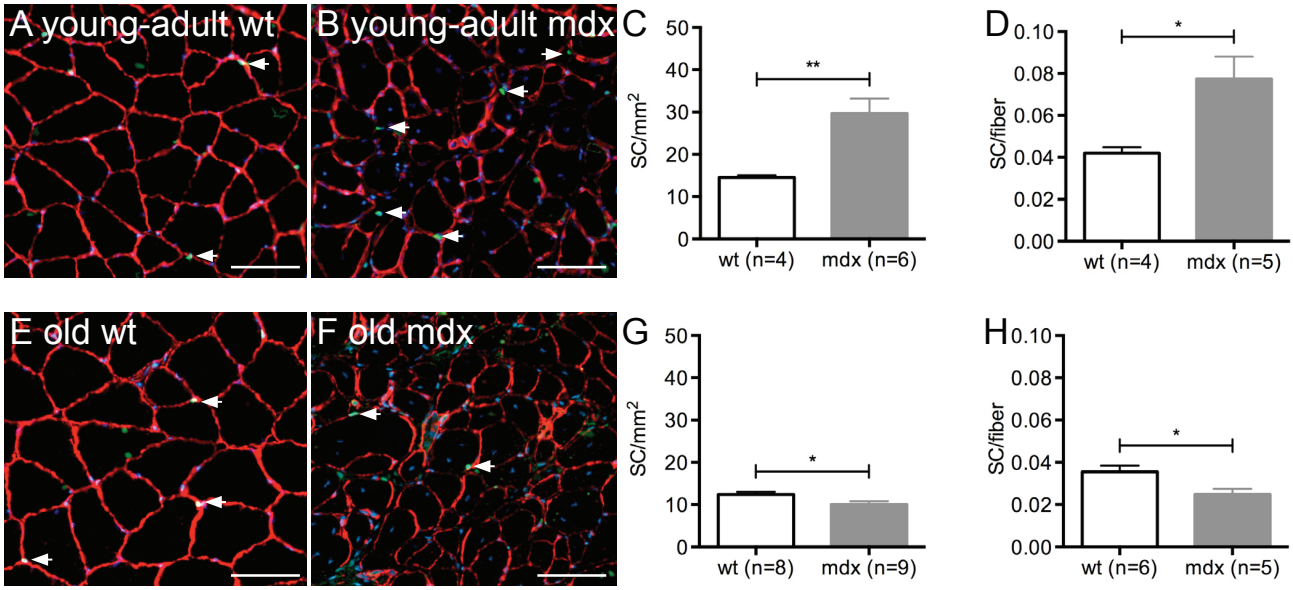

Pericytes and terminal arterioles

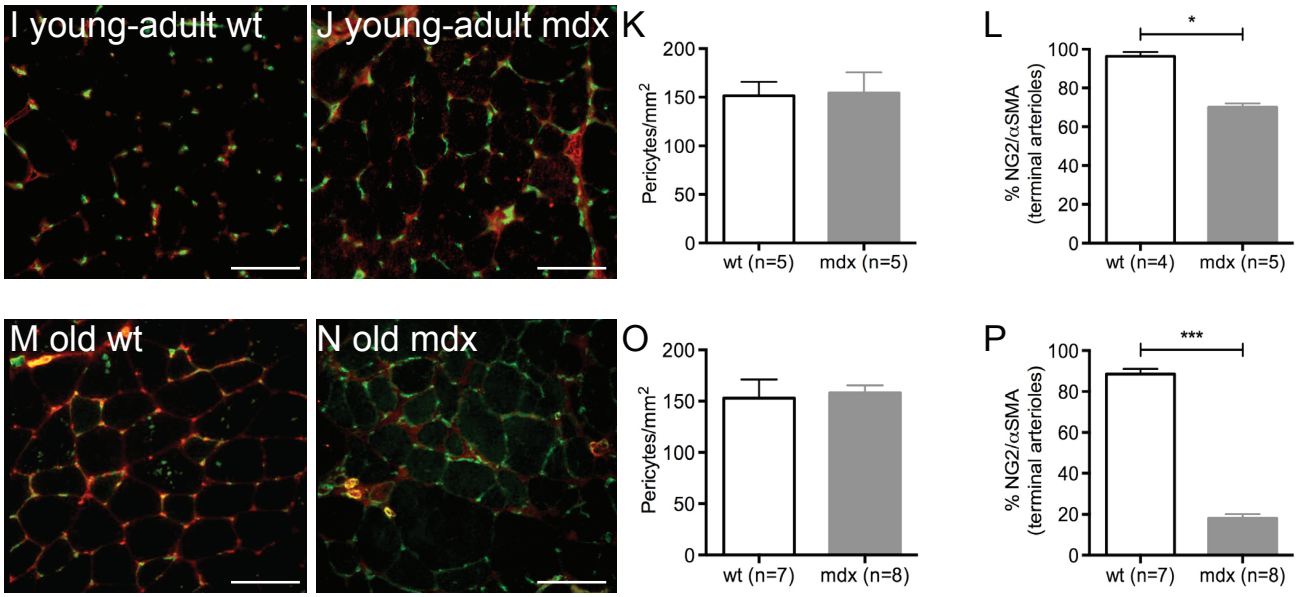

A young adult mdx

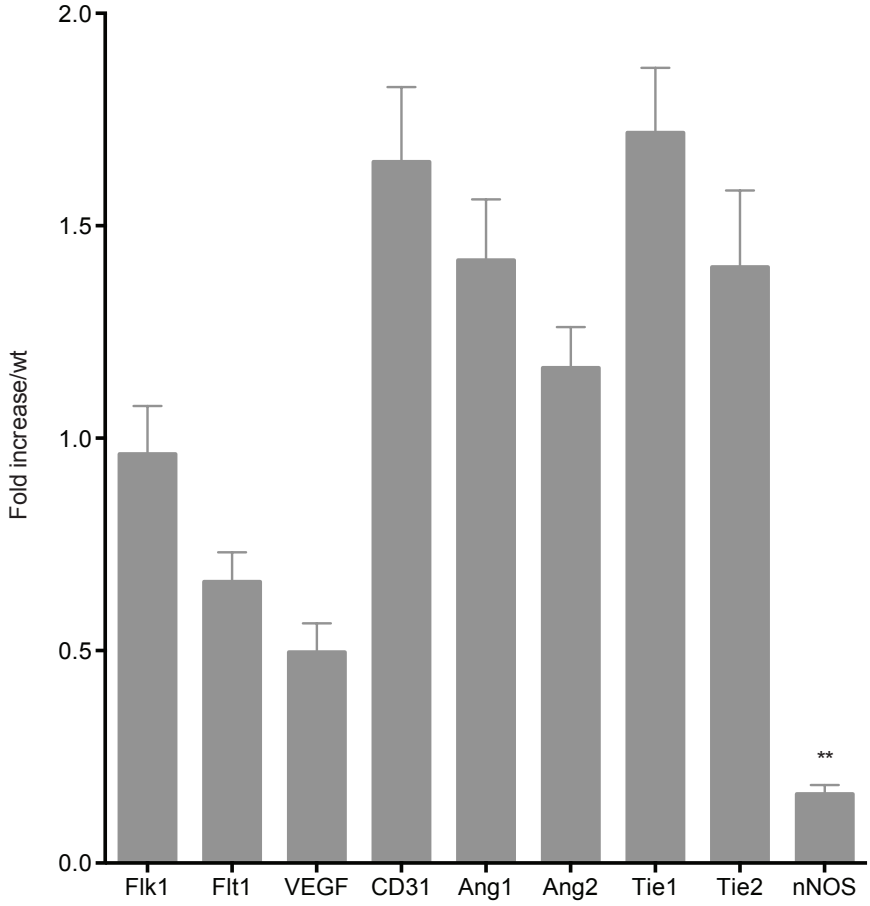

B old mdx

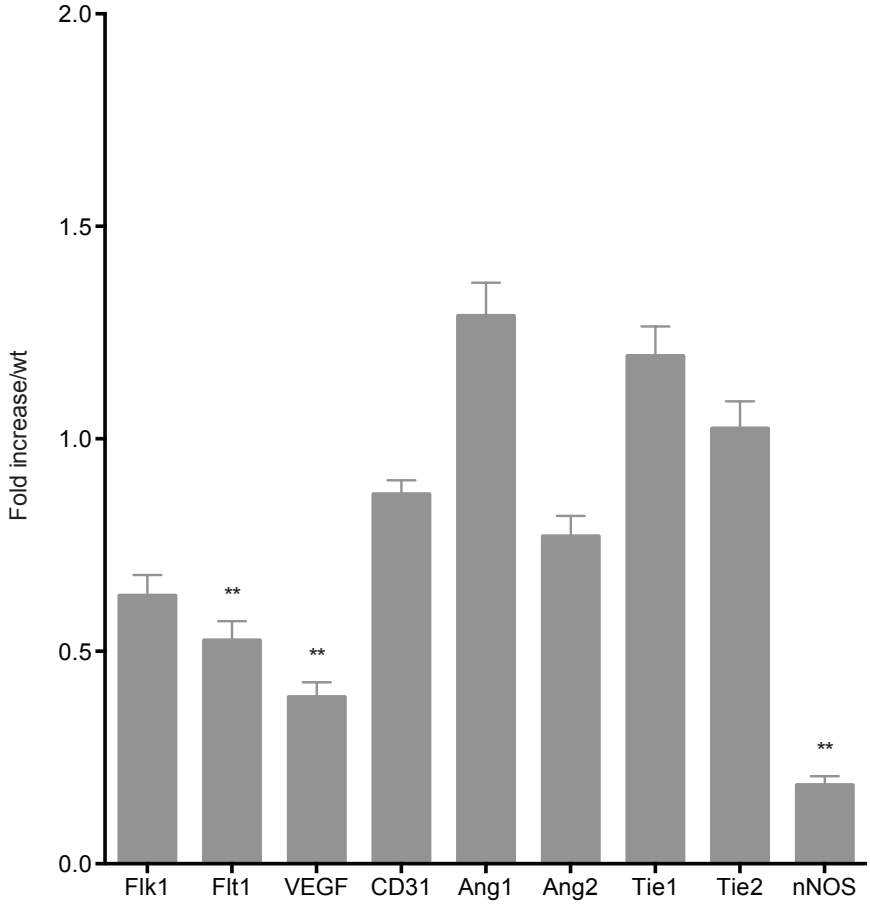

A young adult mice

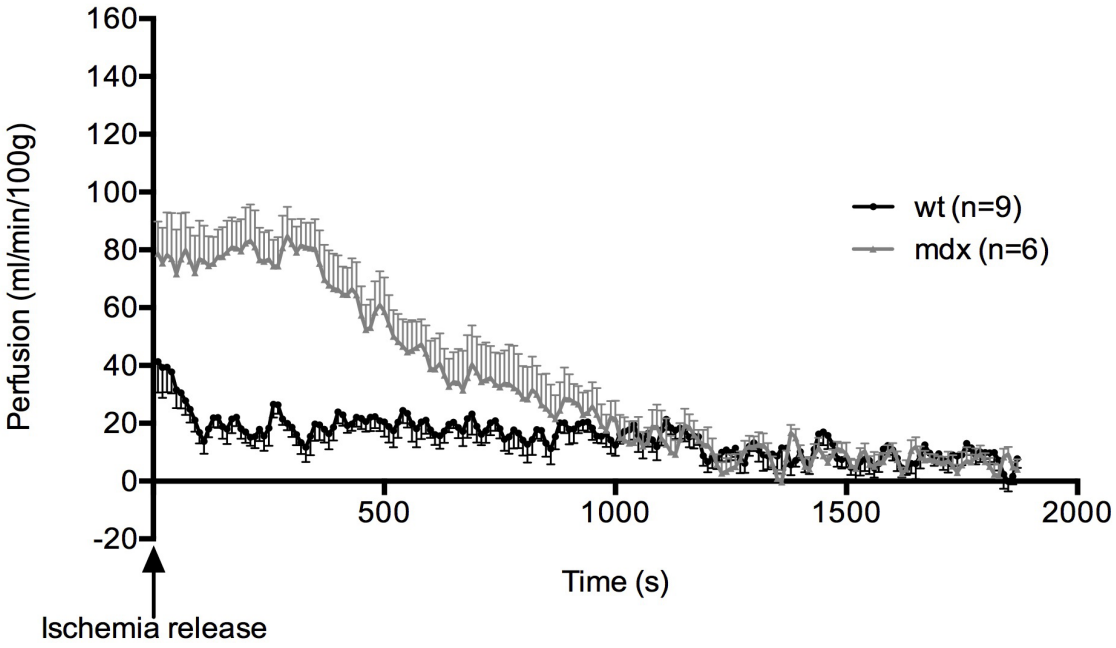

B old mice

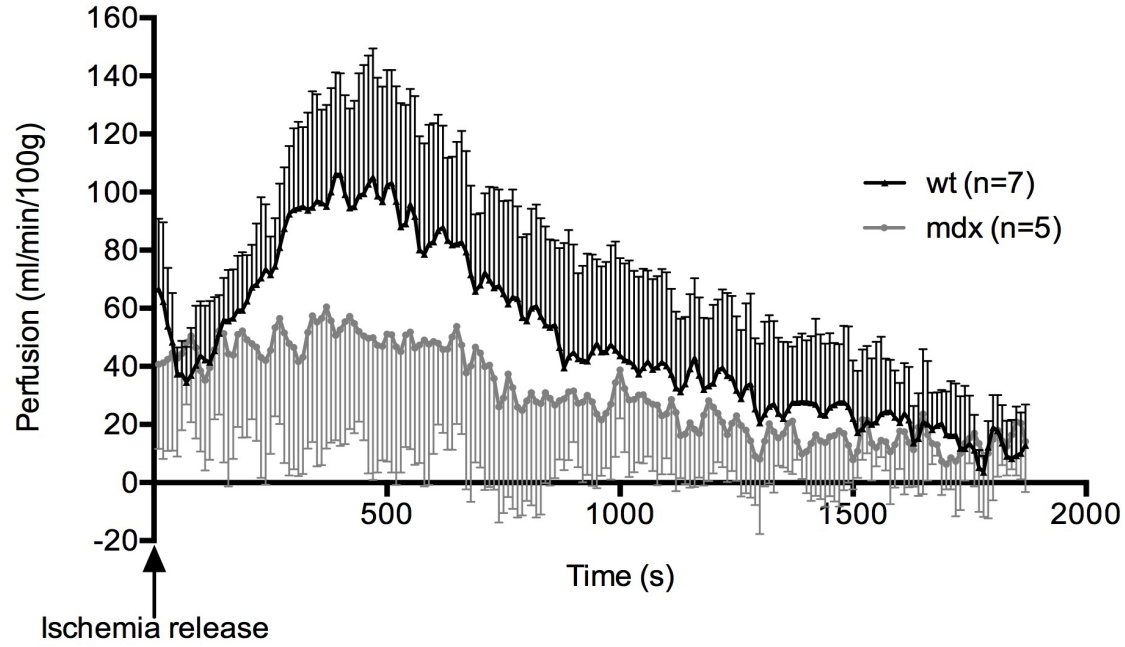

A Correlation maximal perfusion/τPCr

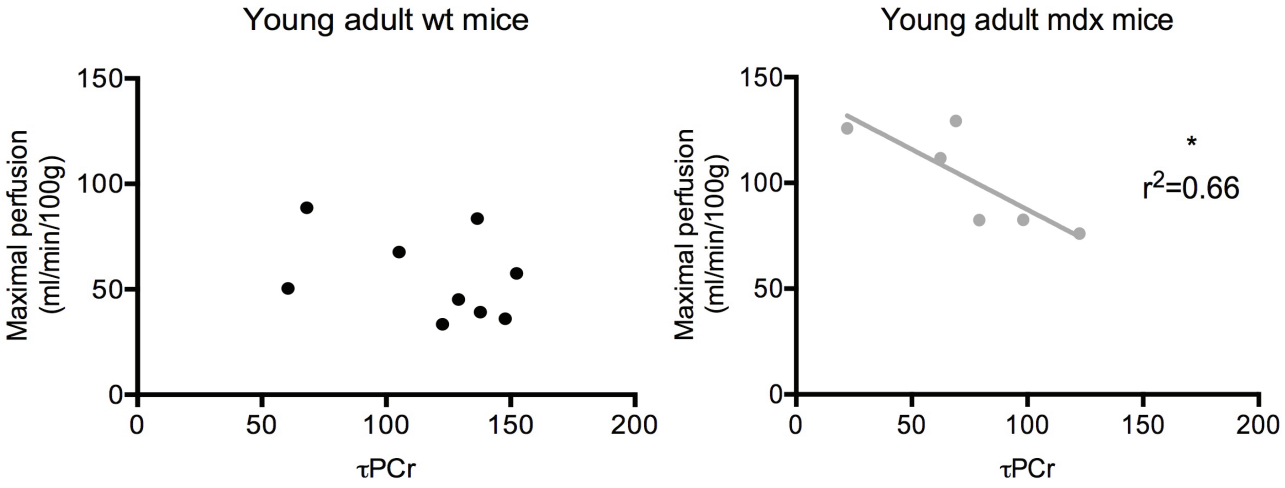

B Correlation perfusion integral until 30 sec/τPCr

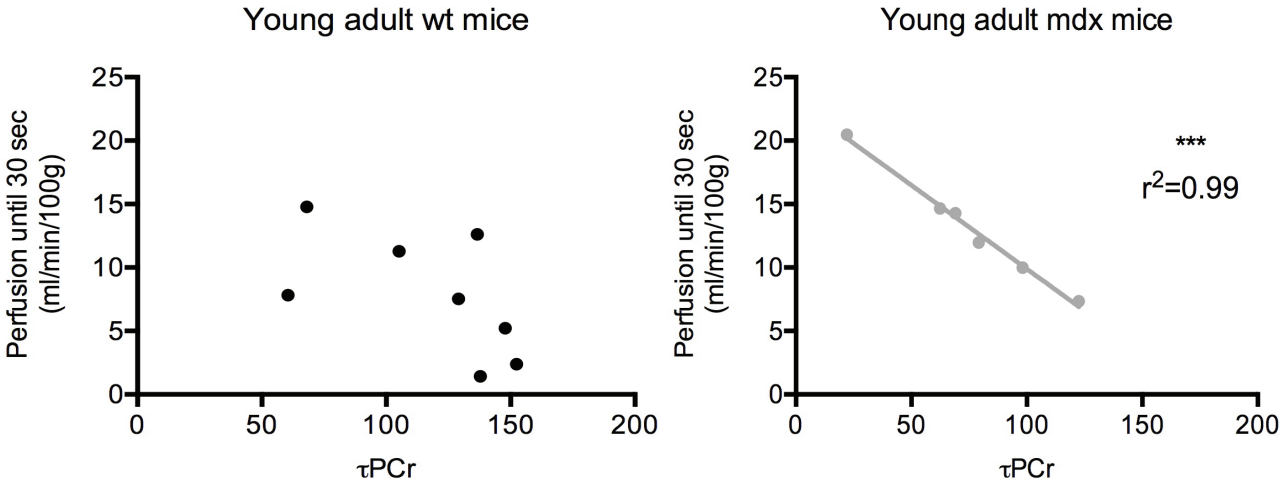

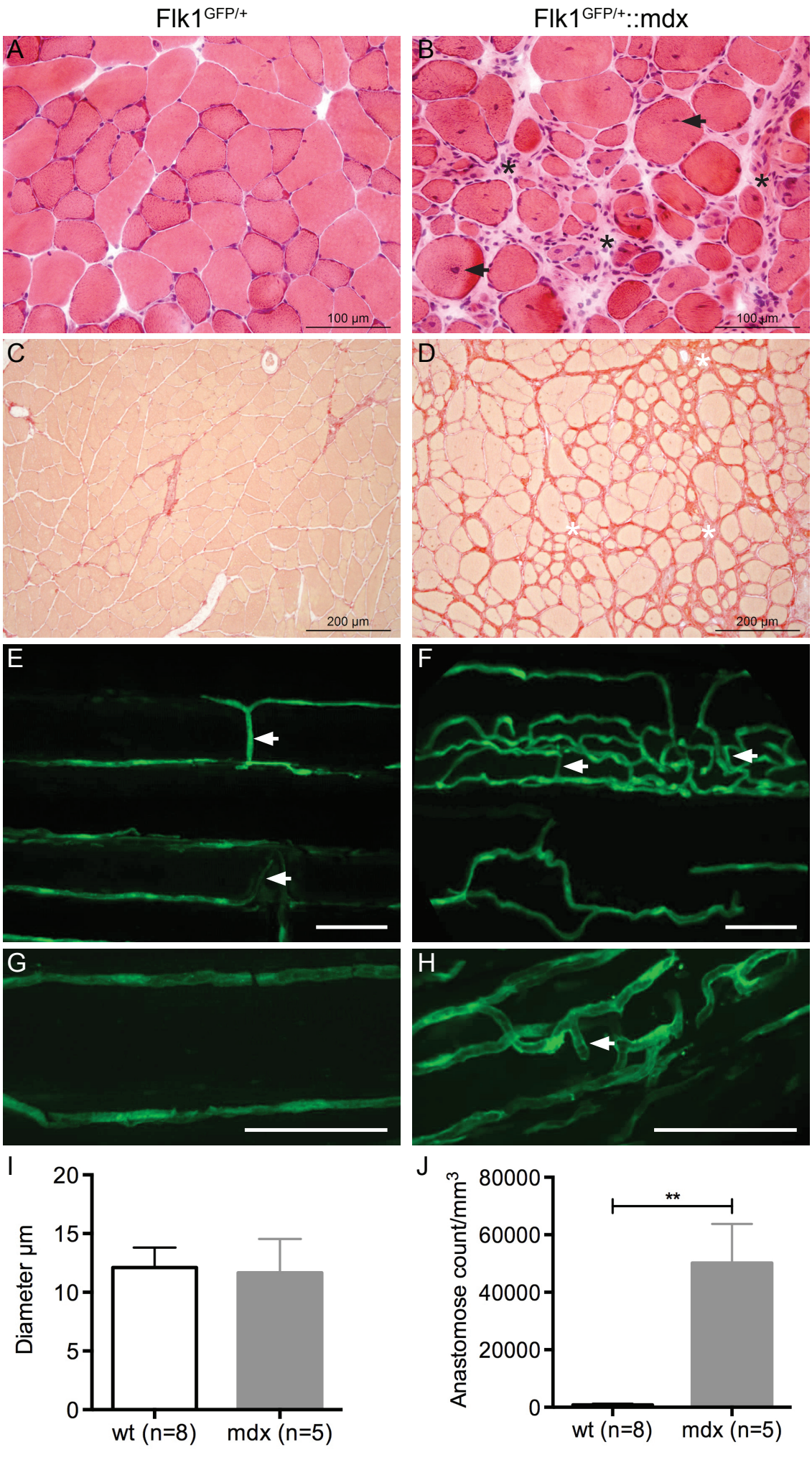
Flk1GFP/+
Flk1GFP/+::mdx
A
B
100 µm
100 µm
C
D
200 µm
200 µm
E
F
G
H
I
Diameter µm
20
15
10
5
0
wt (n=8)
mdx (n=5)
J
Anastomose count/mm3
80000
60000
40000
20000
0
**
wt (n=8)
mdx (n=5)

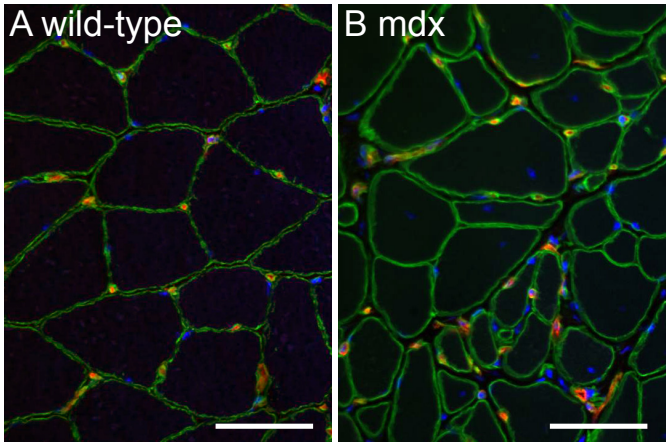
A wild-type
B mdx

C

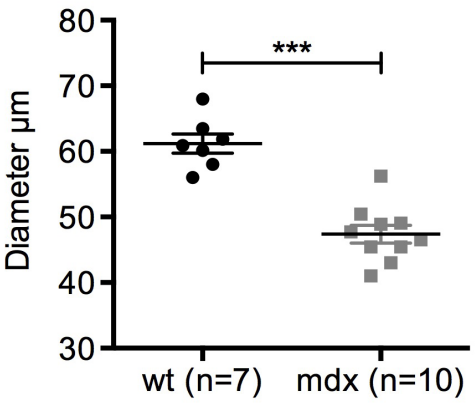
Diameter µm
80
70
60
50
40
30
***
wt (n=7)
mdx (n=10)

D

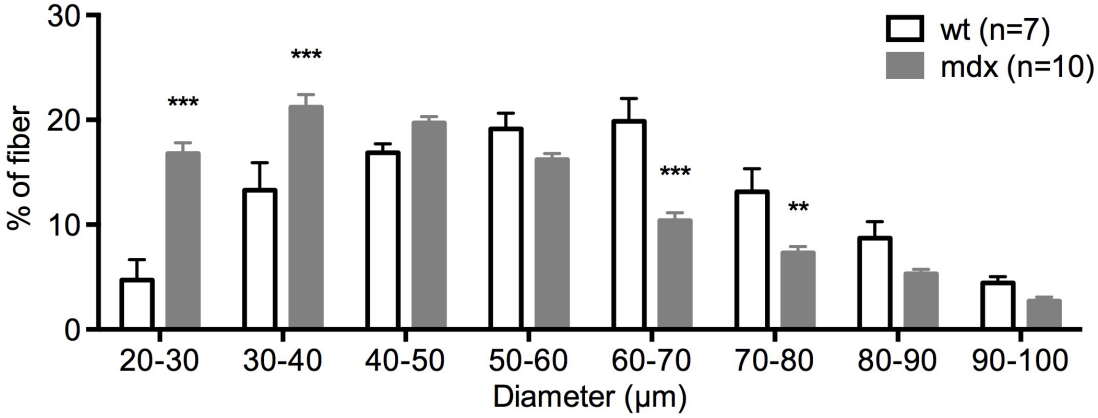
% of fiber
30
20
10
0
***
***
***
**
wt (n=7)
mdx (n=10)
20-30
30-40
40-50
50-60
60-70
70-80
80-90
90-100
Diameter (µm)

E

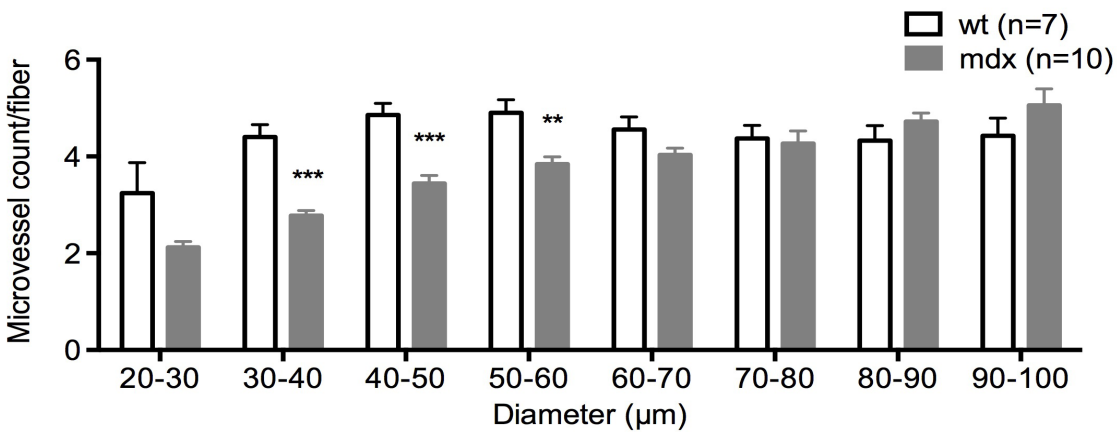
Microvessel count/fiber
6
4
2
0
***
***
**
wt (n=7)
mdx (n=10)
20-30
30-40
40-50
50-60
60-70
70-80
80-90
90-100
Diameter (µm)

F

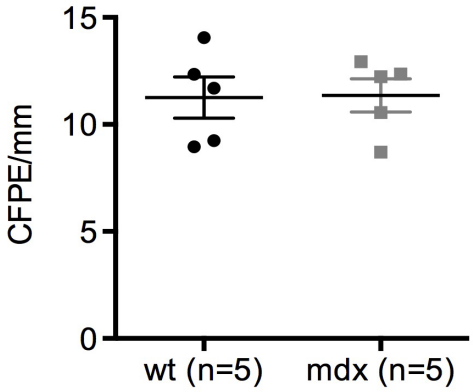
CFPE/mm
15
10
5
0
wt (n=5)
mdx (n=5)

G

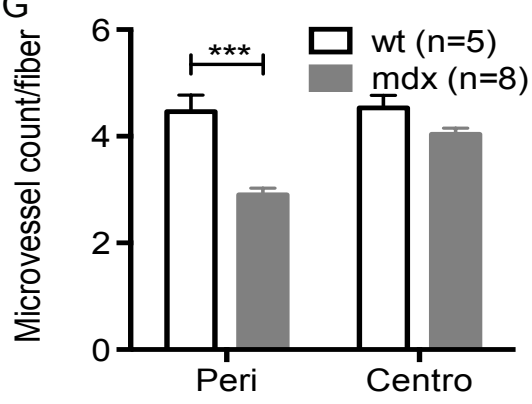
Microvessel count/fiber
6
4
2
0
***
wt (n=5)
mdx (n=8)
Peri
Centro